Research Square

Preprints are preliminary reports that have not undergone peer review.
They should not be considered conclusive, used to inform clinical practice,
or referenced by the media as validated information.

TRIM63-associated signal in sunitinib-resistant xenografts and an eight- gene prognostic score in renal cell carcinoma

Yuyou Deng
Peking University International Hospital
Xiaobing Yang
Peking University International Hospital
Changzhen Hao
Peking University International Hospital
Chengfan Yu
Peking University International Hospital
Ming Xia
Peking University International Hospital
Tian Wang
wangtian2026@126.com
Peking University International Hospital

Research Article

Keywords: Renal cell carcinoma, TRIM63, Sunitinib resistance, Prognostic score, Single-cell RNA sequencing, Spatial transcriptomics

Posted Date: November 5th, 2026

DOI: https://doi.org/10.21203/rs.3.rs-11243781/v1

License: This work is licensed under a Creative Commons Attribution 4.0 International License.
Read Full License

Additional Declarations: No competing interests reported.

Abstract

Background

Sunitinib resistance limits the durable activity of anti-angiogenic therapy in renal cell carcinoma (RCC). This study screened TRIM-family expression in the GSE64052 786-O xenograft model and evaluated a TRIM63-anchored eight-gene risk score (TRIM-8RS) comprising OTX1, LIMCH1, ANK3, TRIM63, CAVIN2, CLTRN, WFDC10B and BBOX1 for prognostic association.

Methods

The score was evaluated in The Cancer Genome Atlas kidney renal clear cell carcinoma (TCGA-KIRC) development cohort (508 patients; 171 deaths) and an independent Clinical Proteomic Tumor Analysis Consortium operational primary-RCC cohort (183 patients; 31 deaths). Model development was repeated with all outcome-dependent candidate screening confined to outer training folds, and discrimination was assessed with Uno's concordance index and inverse-probability-of-censoring-weighted time-dependent receiver operating characteristic analysis.

Results

TRIM63 expression was directionally higher in resistant xenografts, but the association did not survive genome-wide false-discovery-rate adjustment (log2 fold change, 1.84; nominal P = 0.038; adjusted P = 0.291). The apparent Uno concordance index was 0.738 in the development cohort and 0.716 in the external cohort. The 1- and 3-year areas under the curve were 0.804 and 0.745 in TCGA-KIRC and 0.793 and 0.770 in the external cohort, and overall survival differed between risk groups defined by the frozen TCGA median score in both cohorts (hazard ratios, 4.56 and 4.51, respectively). The leakage-controlled reconstruction yielded a mean outer-fold concordance index of 0.699, and multivariable models further adjusted for age, sex and, in TCGA-KIRC, stage and grade. In public single-cell data, TRIM63 was detected in 49 of 17,986 cells, each with one raw unique molecular identifier, and spatial data showed low and variable fractions of TRIM63-positive spots across 11 slides.

Conclusion

These findings support a preliminary prognostic association and further biological validation. They do not establish a causal resistance mechanism or predict clinical benefit.

1 Introduction

Renal cell carcinoma is molecularly heterogeneous. Angiogenic signaling can influence prognosis and response to treatment. Sunitinib, a multi-target tyrosine kinase inhibitor that acts in part through VEGFRs,

improves outcomes in metastatic RCC, but primary and acquired resistance remain common [1, 2]. Resistance can involve angiogenic adaptation, survival signaling, epithelial-mesenchymal plasticity and changes in the tumor microenvironment. Although a signal found in a resistant model is a starting point for testing, its prognostic value must be examined separately from any claim that it predicts treatment benefit.

TRIM proteins are E3 ubiquitin ligases and related regulators with context-dependent effects on cell state, stress responses and cancer biology [3]. TRIM63, also known as MuRF1, is best studied in striated muscle. The behavior of an individual TRIM-family gene can differ with lineage, differentiation state and treatment history. Clear-cell RCC contains distinct molecular and immune states, which makes validation in more than one setting important [4]. Bulk expression data cannot resolve which cells express a candidate gene. Single-cell and spatial transcriptomics can provide cellular and tissue context.

We screened the 786-O sunitinib subgroup of GSE64052 for TRIM-family resistance signals [5, 6]. We then evaluated the historical eight-gene overall-survival score in TCGA-KIRC and CPTAC, while repeating candidate screening and model selection within outer training folds to reduce selection-related optimism. Public ccRCC single-cell and spatial datasets were used to describe sparse TRIM63 detection and compartment-level state scores [7, 8]. This design separates resistance-associated expression, prognostic evaluation and exploratory cellular localization.

The study addressed whether a resistance-clue-anchored expression score showed prognostic association in RCC and whether single-cell and spatial data could provide context for TRIM63 detection. It was not designed to prove causality or predict clinical sunitinib benefit. TCGA-KIRC, GSE152938 and GSE175540 were analyzed as clear-cell RCC resources, whereas CPTAC was analyzed as an operational primary-RCC cohort.

2 Materials and methods

2.1 Study design and data acquisition

This retrospective, multi-cohort transcriptomic study used overall survival (OS) as the primary endpoint. GSE64052 supplied the resistance-associated signal; TCGA-KIRC was used for model training; CPTAC was used for external evaluation; GSE152938 supplied single-cell data for cellular localization and state scoring; and GSE175540 supplied spatial transcriptomic data for an independent detection audit. Analyses used R version 4.4.2. The single-cell and spatial analyses were exploratory because neither dataset contains treatment-response metadata. Spatial transcriptomics was used to assess raw spot-level detection, not to assign cell types or pathological regions. Reporting and interpretation distinguish model development, internal validation and external evaluation, in line with TRIPOD + AI and the bias domains described by PROBAST [9, 10].

2.2 GSE64052 processing and TRIM-family screening

GSE64052, reported by Zhang et al. [6], was downloaded from GEO (platform GPL570; https://www.ncbi.nlm.nih.gov/geo/query/acc.cgi?acc=GSE64052). The primary comparison was fixed before analysis as GSM1563509-GSM1563517, five untreated and four sunitinib-resistant 786-O xenograft tumors. Sorafenib-treated tumors and A498 cell-line samples were excluded. Probes were mapped to genes with the GPL570 annotation, and duplicate mappings were averaged at the gene level. Quantile-normalized expression values were analyzed on the log2 scale, and differential expression was estimated with limma [11]. TRIM40, TRIM63, TRIM38 and TRIM45 were retained to describe the resistance signal. We checked TRIM63 with leave-one-sample-out analyses, Welch tests, Wilcoxon tests and exact label permutations.

2.3 TCGA training cohort and candidate pool

TCGA-KIRC RNA-sequencing TPM and clinical data were obtained from the Genomic Data Commons (https://portal.gdc.cancer.gov/projects/TCGA-KIRC). Primary tumors with evaluable OS formed the development cohort (n = 508; 171 deaths). The original 796-gene GSE64052-linked list and the resistance-screen anchors were retained as the historical input. For the present leakage-free reconstruction, expression filtering, univariable survival screening, fold-local ranking, anchor inclusion and ridge-Cox fitting were performed only in each outer training set. The procedure used 10 repeats of stratified five-fold outer cross-validation, giving 50 held-out folds. No complete-cohort TCGA outcome screen was used to define the fold-local candidate pool.

2.4 Multi-algorithm survival learning and model freezing

The survival outcome was represented as a right-censored pair (T_i, δ_i), where T_i is the observed follow-up time and δ_i in {0,1} indicates death or censoring. For an expression vector x_i, the Cox model is $h(t|x_i) = h_0(t)\exp(\eta_i)$, with $\eta_i=\beta x_i$. Penalized models maximize the partial log-likelihood minus $\lambda * P(\beta)$, with λ selected from training data alone. LASSO-Cox used an L1 penalty for sparse selection. Elastic-net Cox combined L1 and L2 penalties, while ridge regression is the pure L2 case [12]. We used the glmnet R package for LASSO and elastic-net fitting, with internal cross-validation to select the penalty [13].

We compared five survival-learning strategies in each training set: LASSO-Cox, elastic-net Cox, component-wise Cox boosting, random survival forest (RSF) and survival-support-vector-machine (SVM) recursive ranking. LASSO and elastic-net produced penalized linear predictors. Component-wise Cox boosting was implemented with mboost::glmboost and the CoxPH family [14]. RSF used bootstrap trees, random candidate variables at each split and permutation importance [15]. The survival-SVM [16] used a censored ranking loss with a linear kernel, and fold-local variable weights were ranked by absolute value. The algorithms produced ranks of the fold-local preselected genes rather than directly comparable fitted scores. We therefore compared algorithms by held-out discrimination and used rank aggregation across methods and resamples to choose the final genes.

We repeated stratified five-fold outer cross-validation for 10 repeats. In each split, all candidate screening and model selection steps were fitted on the outer training set. The five ranking methods were

LASSO-Cox, elastic-net Cox, component-wise Cox boosting, random survival forest and survival-SVM. The fold-local consensus set was allowed to differ from the historical eight-gene set. Across the 50 consensus resamples, TRIM63 was selected 50 times, OTX1 49 times, LIMCH1 44 times, ANK3 36 times, PLAC1 24 times, WFDC10B 19 times, BBOX1 18 times and CAVIN2 18 times. The redeveloped candidate set was therefore OTX1, LIMCH1, ANK3, TRIM63, PLAC1, WFDC10B, BBOX1 and CAVIN2. A final ridge-Cox model was fit to the full TCGA cohort only after this selection rule was fixed. The historical TRIM-8RS was retained as a locked comparator.

For the historical score, the fixed gene set was OTX1, LIMCH1, ANK3, TRIM63, CAVIN2, CLTRN, WFDC10B and BBOX1, which differs from the nested reconstruction described above. Expression was transformed as log2(TPM + 1) and then converted within each cohort to $z(i,k)=\Phi^{-1}[(\mathrm{rank}(x(i,k)) - 0.5)/n]$, using average ranks for ties. $\text{TRIM-8RS}(i)=\Sigma\,\beta\,z(i,k)$, with frozen ridge-Cox coefficients of 0.3176, − 0.2490, − 0.1231, − 0.0810, − 0.0488, − 0.1234, 0.1169 and − 0.1784 in that gene order (Table 1). The TCGA median score (− 0.099) defined the descriptive high-risk threshold. These rounded coefficients are reported for interpretation; reproducible computation should use the full-precision frozen coefficients in the archived model. The negative TRIM63 coefficient is conditional on the other seven genes and does not change the positive direction of the GSE64052 resistance signal.

For calibration, we retained the TCGA Breslow baseline cumulative hazard after model freezing. At horizon time point t, the predicted event probability was $p(t) = 1-\exp\{-H0,\mathrm{TCGA}(t)*\exp(\text{TRIM-8RS})\}$. In CPTAC, each gene was transformed with an outcome-free within-cohort rank procedure. We did not refit the eight genes, ridge coefficients, TCGA median threshold or TCGA baseline hazard, and did not use CPTAC outcomes to recalibrate them. The score therefore transferred the modeling rule, rather than the TCGA expression scale, across RNA-sequencing platforms.

Table 1
TRIM-8RS risk-score formula and ridge-Cox coefficients.

Gene	Ridge-Cox coefficient (beta)	Role in analysis
OTX1	0.318	Final model gene
LIMCH1	−0.249	Final model gene
ANK3	−0.123	Final model gene
TRIM63	−0.081	GSE64052 resistance-screen anchor
CAVIN2	−0.049	Final model gene
CLTRN	−0.123	Final model gene
WFDC10B	0.117	Final model gene
BBOX1	−0.178	Final model gene

Formula: For patient i and gene k: z(i,k) = inverse_normal_cdf((rank(x(i,k)) − 0.5)/n); TRIM-8RS(i) = sum over k of beta(k) * z(i,k). Here, x(i,k) is the cohort-specific expression of gene k, n is the cohort size, inverse_normal_cdf is the inverse standard-normal cumulative distribution function, and beta(k) is the ridge-Cox coefficient listed above. Coefficients and gene order were frozen before external evaluation.

2.5 Performance evaluation

We summarized discrimination with Uno's inverse-probability-of-censoring-weighted C-index [17] and marginal IPCW time-dependent ROC AUCs at 1 and 3 years [18]. Patient-level nonparametric bootstrap resampling with 1,000 replicates gave 95% intervals for the C-index, AUC and calibration slope. Calibration plots compare quintiles of predicted risk with observed 1-Kaplan-Meier risk. IPCW decision-curve analysis compared TRIM-8RS with treat-all and treat-none strategies over thresholds of 0.05 – 0.60 [19]. Kaplan-Meier groups used the frozen TCGA median score, with Cox models and log-rank tests for separation. TCGA values are apparent development-cohort results unless labeled as outer-fold estimates. Multivariable Cox models tested the score per 1 SD after adjustment for age per 10 years and sex. TCGA models also included grouped AJCC stage and grade. The CPTAC model included age and sex only. The adjusted analyses are summarized in Supplementary Fig. S1.

2.6 CPTAC external validation

CPTAC primary-RCC RNA-sequencing and clinical data were screened through GDC and cBioPortal (https://www.cbioportal.org/study/summary?id=rcc_cptac_gdc). We kept one primary-tumor RNA-sequencing sample per patient under the prespecified audit rule, giving 183 patients and 31 deaths. Gene values were converted with the same outcome-free within-cohort rank procedure, and the frozen TCGA coefficients, median threshold and Breslow baseline hazard were applied without outcome-informed gene selection, coefficient refitting, threshold selection or calibration adjustment. The public diagnosis field was operationally RCC NOS with morphology 8312/3 rather than a uniformly pathology-curated clear-cell diagnosis. We therefore describe CPTAC as an independent operational primary-RCC cohort.

2.7 Single-cell and spatial transcriptomic analyses

We analyzed two public 10x Genomics ccRCC matrices from GSE152938: GSM4630028 (ccRCC1) and GSM4630029 (ccRCC2). Each sample was loaded separately and filtered at nFeature_RNA > 200, nFeature_RNA < 7,000 and mitochondrial RNA fraction < 20%, leaving 8,873 and 9,113 cells. After log-normalization of the data, we selected variable genes, built a graph-based neighborhood structure and calculated UMAP coordinates [20]. The source dataset is reported by Su et al. [7]. Marker modules were used to assign epithelial-like, endothelial-like, pericyte-like, myeloid-like, T/NK-like and mast-like compartments. These labels support localization and stratified summaries instead of pathology-grade annotations.

We transferred the GSE64052 resistant-up and resistant-down signatures to the single-cell matrix and defined the resistance-like score as resistant-up minus resistant-down. Hypoxia and angiogenesis

signature scores were calculated at single-cell resolution using predefined gene sets containing 15 and 19 genes, respectively. UMI counts were normalized using Seurat's LogNormalize method with a scale factor of 10,000, followed by natural-log transformation with a pseudocount of one. For each cell, each signature score was calculated as the unweighted arithmetic mean of the log-normalized expression values of signature genes present in the RNA expression matrix. Zero-expression values were retained, and no control-gene subtraction or gene-wise standardization was applied. Per-cell scores were visualized on UMAP embeddings, and cell-type summaries were calculated as the median score across cells within each annotated compartment.

2.8 Spatial transcriptomic detection audit

We examined all 11 locally available GSE175540 ccRCC spatial transcriptomic slides [8, 21]. For each tissue spot, TRIM63 positivity was defined before analysis as raw UMI > 0, without imputation or smoothing. We summarized the number and fraction of positive tissue spots per slide. The four displayed slides were selected by mean raw TRIM63 UMI per in-tissue spot. For visualization, a per-slide summed-RGB optical-density mask was thresholded by Otsu's method, and at least 0.50 of each circular Visium spot footprint had to overlap the mask. This display mask was a visualization quality-control step, not a pathology annotation. As spatial spots contain multiple cells and pathology regions were unavailable, these data were used only to assess whether sparse TRIM63 detection was present in an independent cohort.

2.9 Statistical analysis and reproducibility

Differential-expression P values were adjusted using the Benjamini-Hochberg method. Unless an adjusted threshold is specified, two-sided $P < 0.05$ was considered nominally significant. Survival analyses used Cox models, Kaplan-Meier curves and log-rank tests. Analysis scripts, processed metadata and frozen-model information are identified in the Data availability statement; original public datasets remain available from their source repositories.

3 Results

3.1 GSE64052 provides a directional TRIM63 resistance signal

The prespecified GSE64052 comparison comprised five untreated and four sunitinib-resistant 786-O animal xenografts. TRIM40 was increased in resistant xenografts (log2 fold change, 2.04; FDR = 0.049), whereas TRIM38 (log2 fold change, − 0.67; FDR = 0.010) and TRIM45 (log2 fold change, − 0.64; FDR = 0.038) were decreased (Fig. 1B-D). TRIM63 was 1.84 log2 units higher in resistant tumors (nominal P = 0.038), but did not meet genome-wide FDR adjustment (FDR = 0.291). The direction of the TRIM63 difference remained positive in all leave-one-sample-out analyses, with estimates ranging from 1.27 to 2.32 log2 units. TRIM63 was therefore retained as a resistance-associated anchor gene for subsequent hypothesis generation, rather than as a confirmed resistance biomarker.

3.2 Historical and nested development of an eight-gene prognostic model

To connect the resistance-associated gene list with patient prognosis, univariable Cox regression analyses were performed in the TCGA-KIRC development cohort, which included 508 primary tumors and 171 deaths. After expression and model-convergence checks, 796 genes were available for analysis. A total of 431 genes showed nominal associations with overall survival at P < 0.05, including 159 genes associated with increased risk and 272 genes associated with reduced risk (Fig. 2A). OTX1 showed the strongest risk association among the leading genes (hazard ratio [HR], 3.04; 95% confidence interval [CI], 2.39 − 3.86; P = 1.34×10^−19), whereas RBM47 showed a protective association (HR, 0.51; 95% CI, 0.43 − 0.61; P = 5.89×10^−15). The forest plot summarized the 20 genes with the smallest nominal P values together with the three prespecified TRIM-family anchors detectable in the TCGA expression matrix. TRIM63 failed to reach nominal significance in the TCGA cohort with an HR of 1.02 (95% CI, 0.86 − 1.21; P = 0.813). TRIM45, TRIM38 and TRIM63 were retained as biologically prespecified anchors because they originated from the GSE64052 resistance screen (Fig. 2B). In a quality-control analysis of 30 randomly selected TCGA tumors, the sample-level median expression across the candidate pool ranged from 1.33 to 3.56 log2(TPM + 1), with interquartile ranges of 2.59 to 4.28 (Fig. 2C). These results defined the input candidate set for subsequent survival-learning analyses.

In the historical analysis, across 50 outer test folds generated by 10 repeated five-fold resampling, the consensus TRIM-8 score achieved a median Uno C-index of 0.693, with a mean of 0.696 and a 2.5th − 97.5th percentile interval of 0.605 − 0.785. The corresponding median C-indices were 0.686 for LASSO-Cox, 0.691 for elastic-net Cox, 0.681 for Cox boosting, 0.692 for random survival forest and 0.689 for survival-SVM (Fig. 3A). The selection-frequency analysis showed substantial heterogeneity in gene selection across the 50 resamples. TRIM63 was retained in all 50 resamples under the prespecified anchor-retention rule, whereas OTX1, LIMCH1 and ANK3 were selected in 49, 40 and 37 resamples, respectively. CAVIN2 was selected in 28 resamples, and CLTRN, WFDC10B and BBOX1 were each selected in 19 resamples (Fig. 3B). The mean fold-local ranking analysis provided a complementary description of algorithm-specific feature prioritization (Fig. 3C). OTX1 generally ranked highly across the algorithms, whereas TRIM63 showed relatively low average ranks despite being retained as an anchor gene. These rankings describe the behavior of the selection procedures across resamples and should not be interpreted as independent evidence of biological importance. In an auxiliary unpenalized Cox model containing all eight genes, LIMCH1 was associated with lower overall mortality (HR, 0.73; 95% CI, 0.60 − 0.90; P = 0.003), whereas OTX1 was associated with higher mortality (HR, 1.45; 95% CI, 1.22 − 1.73; P < 0.001). The remaining genes did not reach nominal statistical significance in this Cox model (Fig. 3D). These hazard ratios were used for descriptive interpretation of individual genes, whereas the deployed TRIM-8RS was defined using ridge-Cox coefficients. Finally, the frozen eight-gene model was evaluated using 1,000 bootstrap resamples with out-of-bag prediction (Fig. 3E). The median out-of-bag Uno C-index was 0.724, with a 2.5th − 97.5th percentile interval of 0.666 − 0.776. The empirical comparison with a non-discriminatory C-index of 0.50 was significant (P < 0.001). Together, these results

indicate that the frozen score showed discrimination under the historical resampling scheme, but that its component selection was heterogeneous and did not satisfy the prespecified stability requirement. Accordingly, the eight-gene score was retained as a preliminary candidate signature for subsequent apparent performance assessment and external evaluation rather than as a definitively stable clinical model. Because the historical candidate pool was screened using full-cohort TCGA outcomes before resampling, these results may retain selection-related optimism. The separate nested reconstruction repeated screening and model fitting within each outer training fold and yielded mean and median outer-fold Uno C-indices of 0.699; it is distinct from the frozen historical score evaluated in CPTAC.

3.3 Apparent TCGA performance of the TRIM-8RS in the TCGA-KIRC training cohort

In the TCGA-KIRC development cohort, the TRIM-8RS showed an Uno C-index of 0.738 (95% CI, 0.696 – 0.777). The time-dependent ROC analysis yielded an AUC of 0.804 (95% CI, 0.748 – 0.857) at 1 year and 0.745 (95% CI, 0.692 – 0.800) at 3 years (Fig. 4A). The continuous risk score was associated with OS, with an HR of 2.25 per 1-SD increase (95% CI, 1.95 – 2.59; P < 0.001). Using the prespecified TCGA median score cutoff of − 0.099, patients in the high-risk group had shorter overall survival than those in the low-risk group (Table 2; HR, 4.56; 95% CI, 3.17 – 6.57; Cox and log-rank P < 0.001; Fig. 4B). In decision-curve analyses, the TRIM-8RS showed positive net benefit across the displayed threshold probabilities of 0.05 – 0.60 for both 1-year and 3-year prediction (Fig. 4C). Quintile-based calibration showed an overall increase in observed risk across groups with increasing predicted risk. For 1-year prediction, mean predicted risk ranged from 0.031 to 0.240 and observed Kaplan–Meier risk ranged from 0.010 to 0.272. For 3-year prediction, the corresponding ranges were 0.085 – 0.518 and 0.075 – 0.524, respectively. The calibration slope was 1.06 (95% CI, 0.88 – 1.28; P = 0.539 versus the ideal value of 1.00; Fig. 4D). These findings represent apparent performance in the TCGA-KIRC development cohort because both the candidate pool and the model were constructed using TCGA data.

Table 2
Clinical characteristics of the TCGA-KIRC development cohort by frozen TRIM-8RS risk group.

Characteristic	Overall (n = 508)	Low risk (n = 254)	High risk (n = 254)	Test	P-value
Age at diagnosis, years, median (IQR)	60.8 (51.8–69.9)	59.7 (49.6–68.6)	62.0 (54.5–72.5)	Wilcoxon rank-sum	0.0040
Sex: Male	338 (66.5%)	157 (61.8%)	181 (71.3%)	Fisher's exact	0.0304
Female	170 (33.5%)	97 (38.2%)	73 (28.7%)		
Vital status at last follow-up: Alive	337 (66.3%)	217 (85.4%)	120 (47.2%)	Fisher's exact	< 0.0001
Dead	171 (33.7%)	37 (14.6%)	134 (52.8%)		
Overall-survival follow-up, days, median (IQR)	1234.0 (619.2–1925.0)	1423.0 (769.5–2175.5)	1094.5 (480.0–1758.0)	Wilcoxon rank-sum	< 0.0001
Pathological grade: G1	9 (1.8%)	9 (3.5%)	0 (0.0%)	Fisher's exact	< 0.0001
G2	188 (37.0%)	127 (50.0%)	61 (24.0%)		
G3	164 (32.3%)	68 (26.8%)	96 (37.8%)		
G4	52 (10.2%)	10 (3.9%)	42 (16.5%)		
GX	1 (0.2%)	0 (0.0%)	1 (0.4%)		
Not reported	94 (18.5%)	40 (15.7%)	54 (21.3%)		
AJCC pathological stage: I/IA/IB	221 (43.5%)	150 (59.1%)	71 (28.0%)	Fisher's exact	< 0.0001
II/IIA/IIB	50 (9.8%)	27 (10.6%)	23 (9.1%)		
III/IIIA/IIIB/IIIC	96 (18.9%)	36 (14.2%)	60 (23.6%)		
IV	56 (11.0%)	8 (3.1%)	48 (18.9%)		
Not reported	85 (16.7%)	33 (13.0%)	52 (20.5%)		

Abbreviations and note: AJCC, American Joint Committee on Cancer; IQR, interquartile range; TRIM-8RS, TRIM63-anchored eight-gene risk score. The TCGA median cutoff was − 0.099; age was available for 474

patients. Values are n (%) or median (IQR). All P values are two-sided Fisher exact or Wilcoxon rank-sum tests. Comparisons of vital status and follow-up after risk grouping are descriptive and are not independent evidence of prognostic performance.

3.4 External evaluation of the historical score

The frozen TRIM-8RS was externally evaluated in the CPTAC operational primary-RCC cohort, comprising 183 patients and 31 deaths. The TCGA-derived gene set, ridge-Cox coefficients, score cutoff and baseline hazard were fixed. The C-index was 0.716 (95% CI, 0.622 – 0.811; P < 0.001 versus 0.50). In inverse-probability-of-censoring-weighted time-dependent ROC analysis, the AUC was 0.793 (95% CI, 0.653 – 0.917) at 1 year and 0.770 (95% CI, 0.644 – 0.879) at 3 years; both estimates were significantly higher than the no-discrimination value of 0.50 (P < 0.001; Fig. 5A). At the fixed TCGA threshold, 96 patients were low risk and 87 were high risk (Table 3). High-risk patients had shorter OS (HR, 4.51; 95% CI, 1.85 – 11.00; log-rank P < 0.001; Fig. 5B). In IPCW decision-curve analysis, the net benefit of TRIM-8RS varied across threshold probabilities from 0.05 to 0.60 and differed according to the prediction horizon (Fig. 5C). Quintile-based calibration showed that observed risk generally increased with increasing predicted risk for both prediction horizons (Fig. 5D). Overall, the TRIM-8RS retained moderate discrimination and risk-stratification ability in the CPTAC cohort. The calibration slope was 1.127 (95% CI, 0.733 – 1.580; P = 0.551 versus 1). The limited event count and broad confidence intervals indicate uncertainty in these external performance estimates.

Table 3 Clinical characteristics of the CPTAC operational primary-RCC RNA-sequencing validation cohort by frozen TRIM-8RS risk group.

Characteristic	Overall (n=183)	Low risk (n=96)	High risk (n=87)	Test	P-value
Age at diagnosis, years, mean±SD	60.1±11.8	59.8±13.1	60.5±10.2	Welch t test	0.7169
Sex: Male	131 (71.6%)	62 (64.6%)	69 (79.3%)	Fisher's exact	0.0331
Female	52 (28.4%)	34 (35.4%)	18 (20.7%)		
Vital status at last follow-up: Alive	152 (83.1%)	90 (93.8%)	62 (71.3%)	Fisher's exact	<0.0001
Dead	31 (16.9%)	6 (6.2%)	25 (28.7%)		
Overall-survival follow-up, days, median (IQR)	1170.0 (443.5–1781.0)	1064.5 (410.8–1772.2)	1175.0 (473.5–1791.0)	Wilcoxon rank-sum	0.5406
Clinical pathological grade	Not available	Not available	Not available	Not tested	NA
Clinical pathological stage	Not available	Not available	Not available	Not tested	NA

Abbreviations: CPTAC, Clinical Proteomic Tumor Analysis Consortium; IQR, interquartile range; NOS, not otherwise specified; RCC, renal cell carcinoma; SD, standard deviation; TRIM-8RS, TRIM63-anchored eight-gene risk score.

Note: Risk groups were assigned using the TCGA median TRIM-8RS threshold: 96 low-risk and 87 high-risk patients. Values are n (%) or mean±SD for age and median (IQR) for follow-up. All tests are two-sided: Fisher exact test for categorical variables, Welch t test for age and Wilcoxon rank-sum test for follow-up. Comparisons of vital status and follow-up after risk grouping are descriptive and are not independent evidence of prognostic performance.

3.5 Single-cell localization of TRIM63 and key signaling pathway score clustering

To examine the cellular distribution of TRIM63, we analyzed two ccRCC single-cell RNA-sequencing datasets, including GSM4630028 (ccRCC1) and GSM4630029 (ccRCC2). After quality-control filtering, 17,986 cells were retained, comprising 8,873 cells from ccRCC1 and 9,113 cells from ccRCC2. Based on marker-based annotation, cells were assigned to epithelial-like, endothelial-like, pericyte-like, myeloid-like, T/NK-like, mast-like and other compartments (Fig. 6A). TRIM63 transcripts were detected in only 49 of the 17,986 cells (0.27%). All TRIM63-positive cells showed low and sparse levels of transcript detection. The positive cells were mainly assigned to the epithelial-like compartment, with additional detections in mast-like, T/NK-like and myeloid-like compartments (Fig. 6B).

We next projected the resistance-like, hypoxia and angiogenesis module scores onto the cellular UMAP embedding (Fig. 6C–E). The resistance-like score was calculated from the difference between the predefined resistant-up and resistant-down gene-set scores. The distributions of these scores varied across the annotated cell types. In summary, the highest median resistance-like scores were observed in endothelial-like and myeloid-like cells, whereas epithelial-like cells showed a lower median score. Epithelial-like cells showed the highest median hypoxia score (1.1343), while endothelial-like cells showed the highest median angiogenesis score (1.2075) (Fig. 6F). These patterns describe compartment-level transcriptional states and do not establish an association between TRIM63 detection and the module scores.

3.6 Spatial distribution of TRIM63 transcripts in ccRCC tissue sections

We further examined the tissue-level distribution of TRIM63 using spatial transcriptomic data from GSE175540. The 11 available tissue sections were ranked according to the mean raw TRIM63 UMI count per in-tissue spot, and the four sections with the highest mean signal were selected for visualization. In the four selected sections, the raw numbers of TRIM63-positive spots were 210 of 4,915 in GSM5924036

(4.27%), 90 of 4,975 in GSM5924033 (1.81%), 75 of 4,562 in GSM5924040 (1.64%), and 51 of 3,829 in GSM5924032 (1.33%) (Fig. 7A–D). Thus, TRIM63-positive spots represented a small fraction of the tissue-associated spots.

These results demonstrate sparse tissue-level detection of TRIM63 transcripts across the selected sections. However, because each spatial spot may contain multiple cells, the maps do not establish spatially restricted sunitinib resistance or a causal relationship between TRIM63 and treatment response.

4 Discussion

The present study identified two main findings. First, TRIM63 showed a directionally higher expression in the sunitinib-resistant 786-O xenografts in GSE64052, although the signal did not survive genome-wide false-discovery-rate adjustment. Second, the historical eight-gene TRIM-8RS was associated with overall survival (OS) in TCGA-KIRC and showed preliminary transportability in the CPTAC operational primary-RCC cohort. The nested reconstruction provided a more appropriate internal assessment after candidate screening was confined to outer training folds. By contrast, the single-cell and spatial analyses showed sparse TRIM63 detection and did not establish a cellular mechanism. Taken together, these findings support further investigation of TRIM63 and TRIM-8RS as hypothesis-generating candidates, but they do not establish causality or predict clinical benefit from sunitinib.

The distinction between model development, internal assessment and external evaluation is important [22]. TCGA-KIRC was the development cohort, and its apparent performance estimates may be optimistic. Feature selection was evaluated using a repeated resampling framework that combined LASSO-Cox, elastic-net Cox, component-wise Cox boosting, random survival forests and survival-SVM. These algorithms were used to compare selection frequency and relative feature ranking across resamples, rather than to define the final clinical score directly. The procedure consisted of 10 repetitions of five-fold resampling, yielding 50 outer test folds. TRIM63 was selected in all 50 resamples; however, it was prespecified as a biological anchor and subject to an anchor-retention rule, so this frequency should not be interpreted as fully data-driven selection stability. The historical score showed OS stratification in TCGA-KIRC and CPTAC, but prognostic association should not be interpreted as evidence of treatment-benefit prediction. Demonstrating benefit prediction would require treatment allocation, response or progression data and a treatment-by-score interaction analysis. In CPTAC, the C-index of 0.716 and the 1- and 3-year AUCs of 0.793 and 0.770 support broadly consistent risk ranking across the evaluated horizons, but 31 deaths and the resulting wide confidence intervals preclude a claim of precise or clinically established stability.

TRIM63 was prioritized because its expression was higher in the resistant xenograft comparison, the direction of the estimate remained positive in leave-one-sample-out analyses, and it was the only TRIM-family anchor retained in the historical score. These features provide a rationale for follow-up, but the small xenograft comparison and the absence of a nominal TCGA OS association limit mechanistic inference. The negative TRIM63 coefficient in the multivariable historical score is conditional on the

other seven genes and should not be interpreted as evidence that TRIM63 is protective or suppresses resistance. Independent pathology work has reported TRIM63 as a diagnostic biomarker in MiT family aberration-associated RCC [23], but that diagnostic context is distinct from the present hypothesis about sunitinib resistance in ccRCC.

The single-cell analyses showed that resistance-like, hypoxia and angiogenesis module scores varied across annotated compartments. These scores describe expression of predefined gene sets. The resistance-like score is also distinct from the eight-gene TRIM-8RS and is not a measured treatment-response label. The observed cell-type differences are therefore descriptive and do not demonstrate that TRIM63 drives these transcriptional states.

The spatial analysis provides a complementary tissue-level view but has similar interpretive limits. TRIM63-positive spots were observed across the audited slides, while their proportions varied substantially. Because a spatial spot may contain multiple cells, these maps cannot identify the expressing cell type or define a pathological tumor region. RNA in situ validation, higher-resolution cellular assays and direct perturbation experiments are needed to clarify the source and biological significance of the signal.

The principal limitations are the small animal xenograft comparison, the limited CPTAC death-event count and the retrospective use of public datasets. The external cohort contained 31 deaths, which limits the precision of discrimination, calibration and decision-curve estimates. Sample-size requirements for external validation of time-to-event prediction models depend on the expected predictor distribution, event and censoring distributions and the target precision of calibration and discrimination estimates [24]; therefore, the present CPTAC analysis should be viewed as preliminary rather than definitive. The single-cell and spatial analyses were sparse-detection audits, and each spatial spot may contain multiple cells. Direct TRIM63 perturbation, higher-coverage cellular validation, RNA in situ confirmation and treatment-response cohorts will be required before mechanistic or clinical claims can be made.

5 Conclusions

GSE64052 provides a directionally positive but statistically limited TRIM63 signal in a 786-O sunitinib-resistant xenograft model. The historical TRIM-8RS was associated with OS in TCGA-KIRC and showed preliminary external prognostic performance in CPTAC. The nested reconstruction yielded a mean outer-fold Uno C-index of 0.699. Sparse single-cell and spatial detection does not establish a malignant-cell program or treatment-response effect. TRIM63 and TRIM-8RS warrant further validation, but neither is established here as a clinical predictor of sunitinib benefit.

Abbreviations

AJCC, American Joint Committee on Cancer; AUC, area under the curve; ccRCC, clear-cell renal cell carcinoma; CI, confidence interval; CPTAC, Clinical Proteomic Tumor Analysis Consortium; FDR, false

discovery rate; GEO, Gene Expression Omnibus; HR, hazard ratio; IPCW, inverse probability of censoring weighting; KIRC, kidney renal clear cell carcinoma; OS, overall survival; RCC, renal cell carcinoma; RSF, random survival forest; SD, standard deviation; SVM, support vector machine; TCGA, The Cancer Genome Atlas; TPM, transcripts per million; TRIM-8RS, TRIM63-anchored eight-gene risk score; UMAP, uniform manifold approximation and projection; UMI, unique molecular identifier; VEGFR, vascular endothelial growth factor receptor.

Declarations

Acknowledgements

The authors thank the investigators and participants who generated the public GEO, TCGA and CPTAC resources used in this study.

Author contributions

Yuyou Deng: conceptualization, data curation, formal analysis, investigation, methodology, software, writing—original draft. Xiaobing Yang: data curation, investigation, methodology. Changzhen Hao: data curation, investigation, methodology, software. Chengfan Yu: supervision, validation. Ming Xia: supervision, validation. Tian Wang: conceptualization, supervision, validation, writing—review and editing. All authors interpreted the findings, revised the manuscript, and read and approved the final version. Tian Wang and Yuyou Deng confirm the authenticity of the raw data.

Funding

This research was supported by the Peking University International Hospital In-Hospital Research Fund, under Grant No. YN2024QX02.

Data availability

The GEO series GSE64052 is available at https://www.ncbi.nlm.nih.gov/geo/query/acc.cgi?acc=GSE64052. The single-cell matrices are available under GEO accession GSE152938 (GSM4630028 and GSM4630029), and the spatial-transcriptomic matrices are available under GEO accession GSE175540. TCGA-KIRC data are available through the Genomic Data Commons at https://portal.gdc.cancer.gov/projects/TCGA-KIRC. CPTAC-3 Kidney resources are available through https://portal.gdc.cancer.gov/projects/CPTAC-3 and the cBioPortal study page at https://www.cbioportal.org/study/summary?id=rcc_cptac_gdc. The GitHub repository is https://github.com/tkvillage/TRIM-63-anchored-prognostic-model-in-sunitinib-resistant-ccRCC; its archived release is available through Zenodo at https://doi.org/10.5281/zenodo.22168259. Analysis

scripts, processed input metadata, clinical-screening audits, fold-level results and model coefficients are preserved in the project repository and archived release. No individual-level controlled-access data are redistributed in this manuscript package.

Ethics approval and consent to participate

The study used de-identified, publicly available datasets and involved neither new human-specimen collection nor intervention. Institutional ethics approval and consent to participate were therefore not required for this secondary analysis.

Consent for publication

Not applicable; no identifiable individual-level information is reported.

Competing interests

The authors declare that they have no competing interests.

Use of artificial intelligence tools

Generative artificial-intelligence tools assisted with language editing, manuscript organization, literature-search support and document formatting. No new experimental observations or patient data were generated during manuscript revision. The authors are responsible for checking all citations, numerical results and scientific interpretations and for approving the final manuscript.

References

1. Motzer RJ, Hutson TE, Tomczak P, et al. Sunitinib versus interferon alfa in metastatic renal-cell carcinoma. N Engl J Med. 2007;356:115–24.
2. Butz H, Ding Q, Nofech-Mozes R, Lichner Z, Ni H, Yousef GM, et al. Elucidating mechanisms of sunitinib resistance in renal cancer: an integrated pathological-molecular analysis. Oncotarget. 2018;9:4661–74.
3. Hatakeyama S. TRIM proteins and cancer. Nat Rev Cancer. 2011;11:792–804.
4. Cancer Genome Atlas Research Network. Comprehensive molecular characterization of clear cell renal cell carcinoma. Nature. 2013;499:43–9.
5. Edgar R, Domrachev M, Lash AE. Gene Expression Omnibus: NCBI gene expression and hybridization array data repository. Nucleic Acids Res. 2002;30:207–10.

6. Zhang L, Wang X, Bullock AJ, Callea M, Shah H, Song J, et al. Anti-S1P antibody as a novel therapeutic strategy for VEGFR TKI-resistant renal cancer. Clin Cancer Res. 2015;21:1925–34. 10.1158/1078-0432.CCR-14-2031.
7. Su C, Lv Y, Lu W, Yu Z, Ye Y, Guo B, et al. Single-cell RNA sequencing in multiple pathologic types of renal cell carcinoma revealed novel potential tumor-specific markers. Front Oncol. 2021;11:719564.
8. Meylan M, Petitprez F, Becht E, Bougoüin A, Pupier G, Calvez A et al. Tertiary lymphoid structures generate and propagate anti-tumor antibody-producing plasma cells in renal cell cancer. Immunity. 2022;55:527 – 541.e5.
9. Collins GS, Moons KGM, Dhiman P, Riley RD, Beam AL, Van Calster B, et al. TRIPOD + AI statement: updated guidance for reporting clinical prediction models that use regression or machine learning methods. BMJ. 2024;385:e078378. 10.1136/bmj-2023-078378.
10. Wolff RF, Moons KG, Riley RD, Whiting PF, Westwood M, Collins GS, et al. PROBAST: a tool to assess the risk of bias and applicability of prediction model studies. Ann Intern Med. 2019;170:51–8.
11. Ritchie ME, Phipson B, Wu D, Hu Y, Law CW, Shi W, et al. limma powers differential expression analyses for RNA-sequencing and microarray studies. Nucleic Acids Res. 2015;43:e47.
12. Hoerl AE, Kennard RW. Ridge regression: biased estimation for nonorthogonal problems. Technometrics. 1970;12:55–67.
13. Simon N, Friedman J, Hastie T, Tibshirani R. Regularization paths for Cox's proportional hazards model via coordinate descent. J Stat Softw. 2011;39:1–13.
14. Hothorn T, Buehlmann P, Kneib T, Schmid M, Hofner B. Model-based boosting 2.0. J Mach Learn Res. 2010;11:2109–13.
15. Ishwaran H, Kogalur UB, Blackstone EH, Lauer MS. Random survival forests. Ann Appl Stat. 2008;2:841–60.
16. Van Belle V, Pelckmans K, Van Huffel S, Suykens JAK. Improved performance on high-dimensional survival data by application of survival-SVM. Bioinformatics. 2011;27:87–94. 10.1093/bioinformatics/btq617.
17. Uno H, Cai T, Pencina MJ, D'Agostino RB, Wei LJ. On the C-statistics for evaluating overall adequacy of risk prediction procedures with censored survival data. Stat Med. 2011;30:1105–17.
18. Blanche P, Dartigues JF, Jacqmin-Gadda H. Estimating and comparing time-dependent areas under receiver operating characteristic curves for censored event times with competing risks. Stat Med. 2013;32:5381–97.
19. Vickers AJ, Elkin EB. Decision curve analysis: a novel method for evaluating prediction models. Med Decis Mak. 2006;26:565–74.
20. Stuart T, Butler A, Hoffman P, Hafemeister C, Papalexi E, Mauck WM 3. rd, Comprehensive integration of single-cell data. Cell. 2019;177:1888 – 1902.e21.
21. Ståhl PL, Salmén F, Vickovic S, Lundmark A, Navarro JF, Magnusson J, et al. Visualization and analysis of gene expression in tissue sections by spatial transcriptomics. Science. 2016;353:78–82.

10.1126/science.aaf2403.

22. Ramspek CL, Jager KJ, Dekker FW, Zoccali C, van Diepen M. External validation of prognostic models: what, why, how, when and where? Clin Kidney J. 2021;14:49–58.
23. Wang XM, Zhang Y, Mannan R, Skala SL, Rangaswamy R, Chinnaiyan A, et al. TRIM63 is a sensitive and specific biomarker for MiT family aberration-associated renal cell carcinoma. Mod Pathol. 2021;34:1596–607. 10.1038/s41379-021-00803-z.
24. Riley RD, Collins GS, Ensor J, Archer L, Booth S, Mozumder SI, et al. Minimum sample size calculations for external validation of a clinical prediction model with a time-to-event outcome. Stat Med. 2022;41:1280–95. 10.1002/sim.9275.

Figures

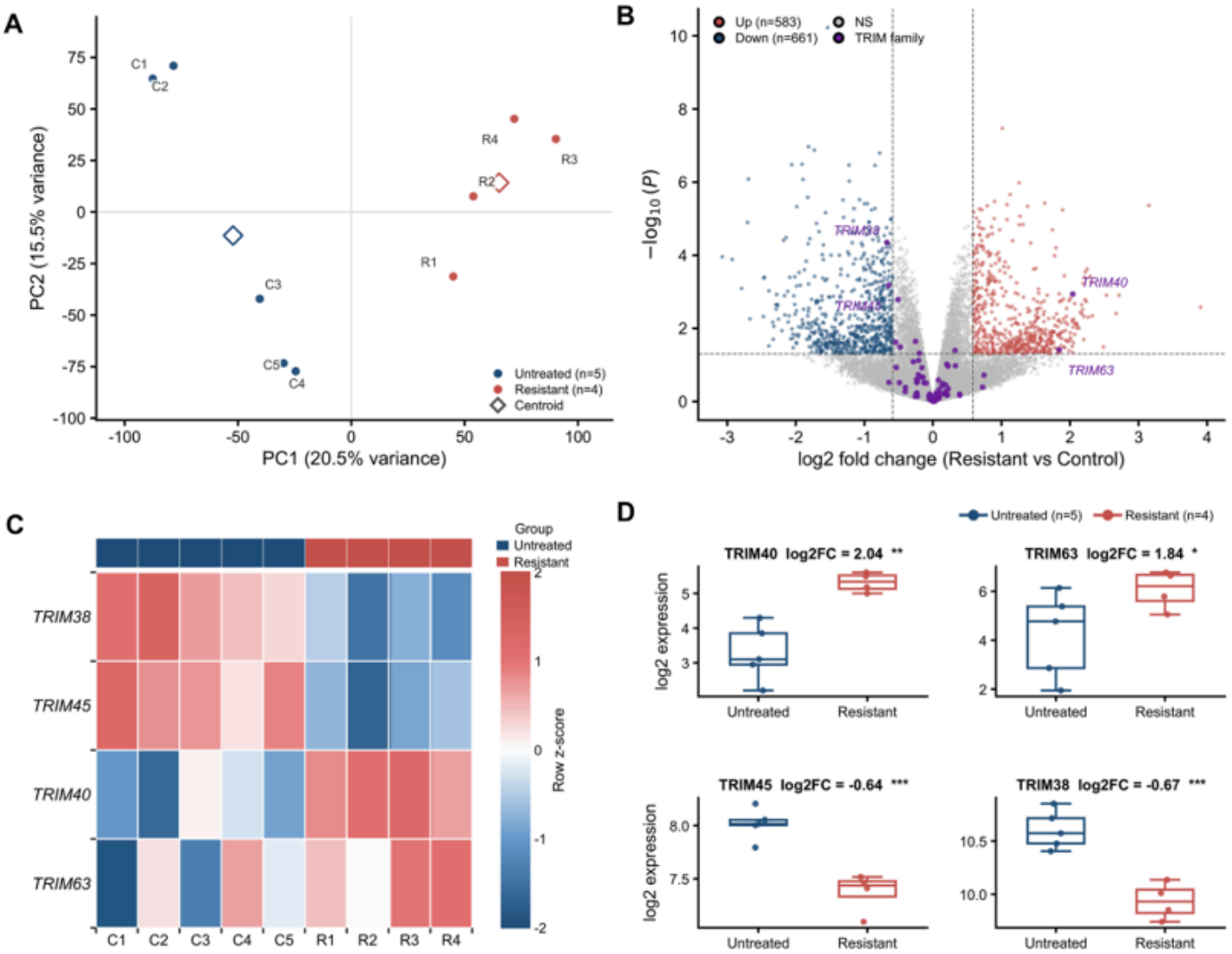


Figure 1

GSE64052 786-O xenograft resistance screen. A Principal-component analysis of quantile-normalized log2 expression in the prespecified subgroup of five untreated tumors (C1-C5; GSM1563509-GSM1563513) and four sunitinib-resistant tumors (R1-R4; GSM1563514-GSM1563517). Expression values for 21,452 gene symbols were centered and scaled across samples. B limma volcano plot for resistant versus untreated xenografts. At the displayed nominal criteria of P<0.05 and absolute log2 fold change >0.585, 583 genes were upregulated and 661 were downregulated. Purple points identify TRIM-family genes, and the four nominally altered TRIM genes are labeled. C Row z-score heat map of TRIM38, TRIM45, TRIM40 and TRIM63 across the nine xenografts. D Individual expression values for these genes. Resistant-versus-untreated log2 fold changes were 2.04 for TRIM40, 1.84 for TRIM63, −0.64 for TRIM45 and −0.67 for TRIM38. TRIM63 had a nominal limma P value of 0.038 but a Benjamini-Hochberg false-discovery rate of 0.291 across 21,452 genes. This small xenograft comparison therefore provides a directional resistance clue, not a clinically validated resistance biomarker. *P<0.05, **P<0.01 and ***P<0.001. Data source: GEO series GSE64052 [5, 6].

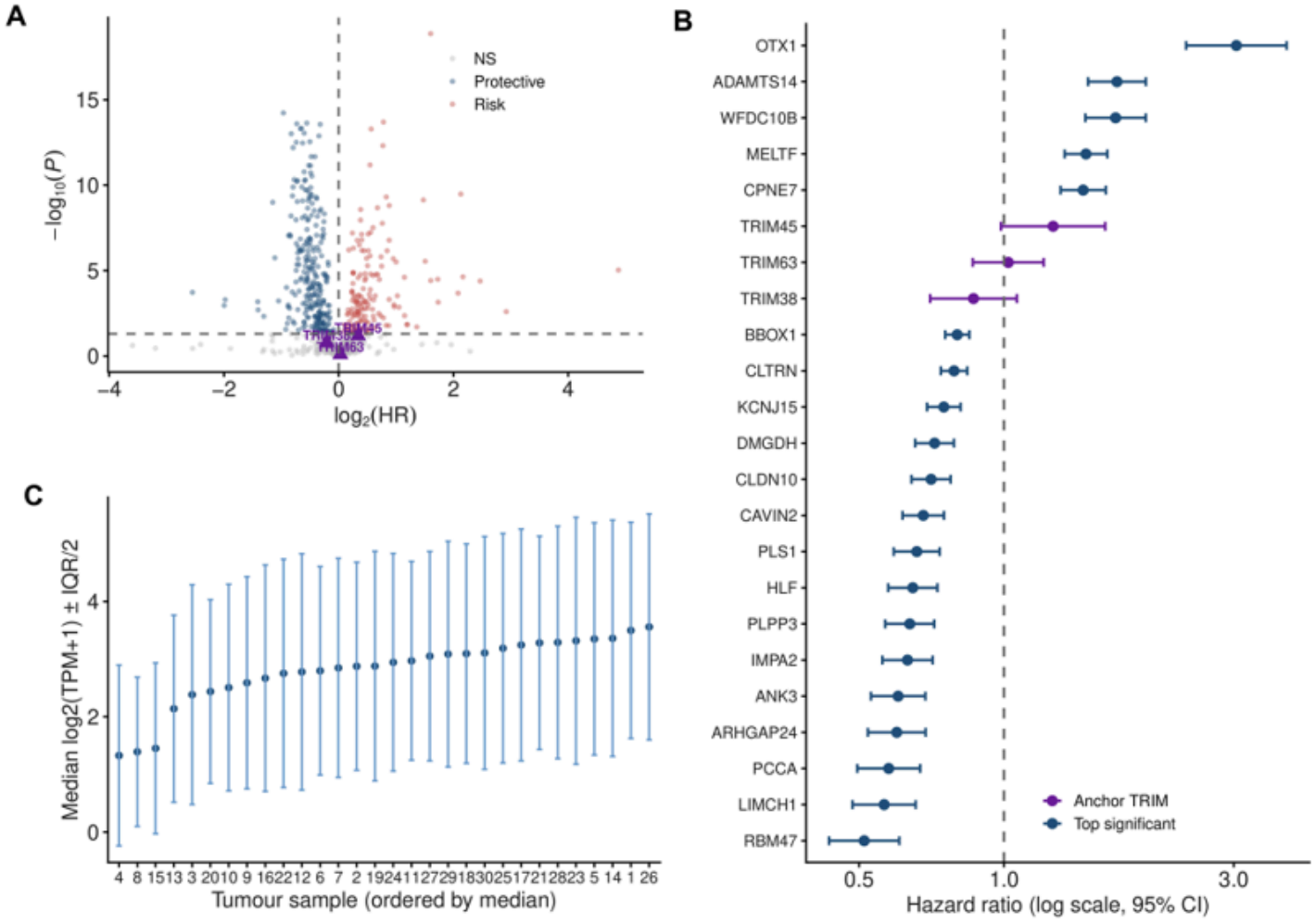


Figure 2

Historical candidate-pool generation in the TCGA-KIRC development cohort. A Univariable overall-survival screen of 796 GSE64052-linked genes. Points show log2 hazard ratios against −log10 nominal P

values; 431 genes met nominal P<0.05. Purple triangles identify the resistance-screen anchors TRIM63, TRIM38 and TRIM45. B Hazard ratios and 95% confidence intervals for the 20 genes with the smallest nominal P values and the three anchors. The dashed line denotes a hazard ratio of 1. C Expression quality-control display for the 796-gene candidate pool in 30 randomly sampled TCGA tumors. Points indicate within-sample medians and bars indicate half interquartile ranges of log2(TPM+1). The full-cohort outcome screen preceded historical resampling and is shown to document a potential source of optimism. It did not constitute the fold-local candidate selection used for the leakage-free reconstruction. Data source: TCGA-KIRC, Genomic Data Commons.

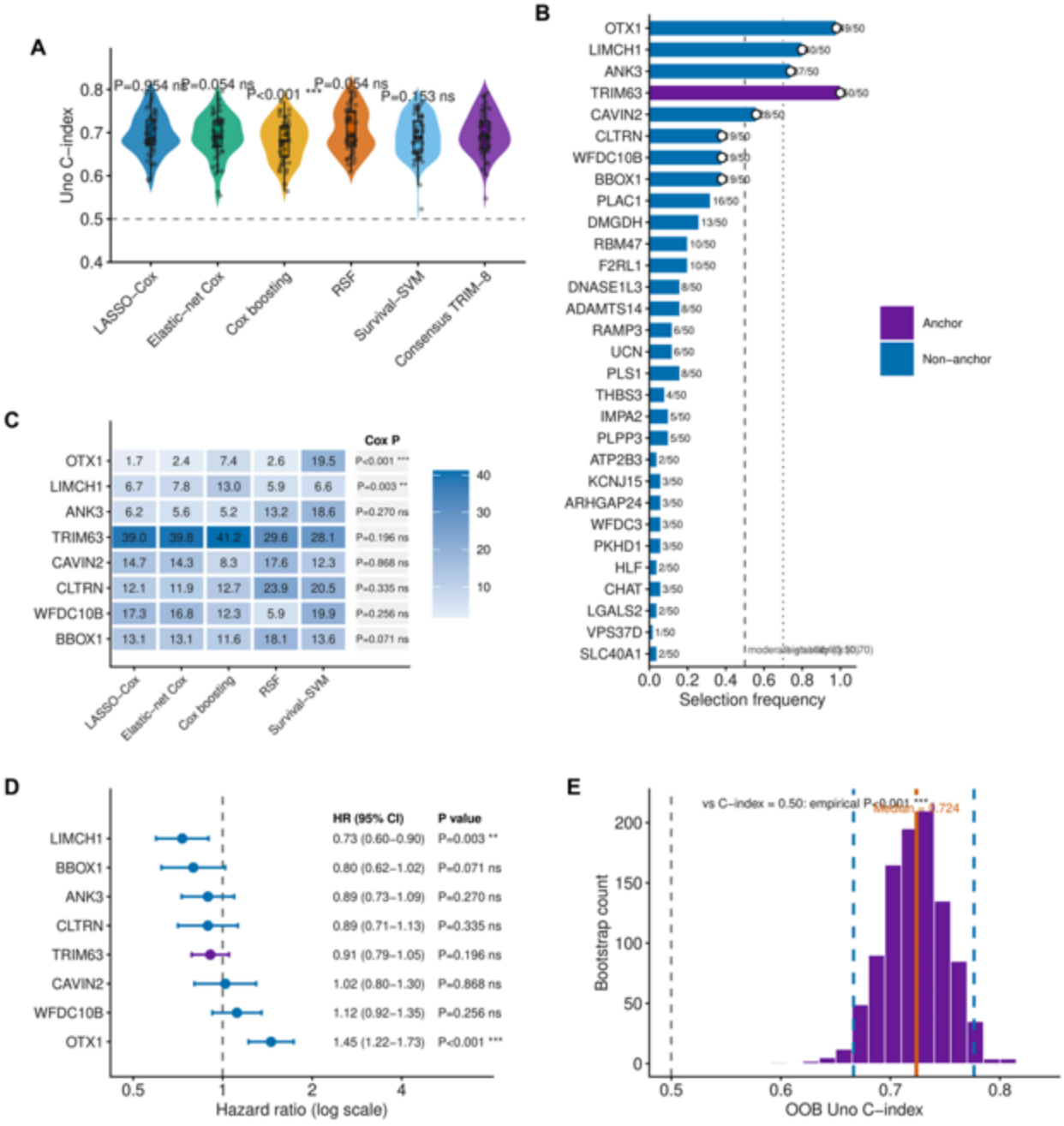


Figure 3

Historical resampling analysis for the frozen eight-gene TRIM-8RS. A Distributions of outer-test-fold Uno C-indices for LASSO-Cox, elastic-net Cox, component-wise Cox boosting, random survival forest, survival support-vector machine and the consensus TRIM-8 set across 50 held-out folds. Labels show Benjamini-Hochberg-adjusted paired Wilcoxon P values versus the consensus set. B Selection frequencies for the 30 leading candidates across 50 resamples. Purple bars identify resistance anchors, and open circles mark genes retained in the historical eight-gene score. C Mean fold-local feature ranks for the historical score genes across the five algorithms; the adjacent column gives auxiliary Cox P values. D Auxiliary unpenalized Cox hazard ratios, 95% confidence intervals and P values for the same genes. The deployed historical score used ridge-Cox coefficients. E Out-of-bag Uno C-index distribution from 1,000 bootstrap replicates; the median was 0.724 and the empirical P value versus 0.50 was <0.001. Because the candidate pool was outcome-prefiltered before these resamples, this figure is a historical comparator. It does not represent the separate leakage-free reconstruction. Data source: TCGA-KIRC, Genomic Data Commons.

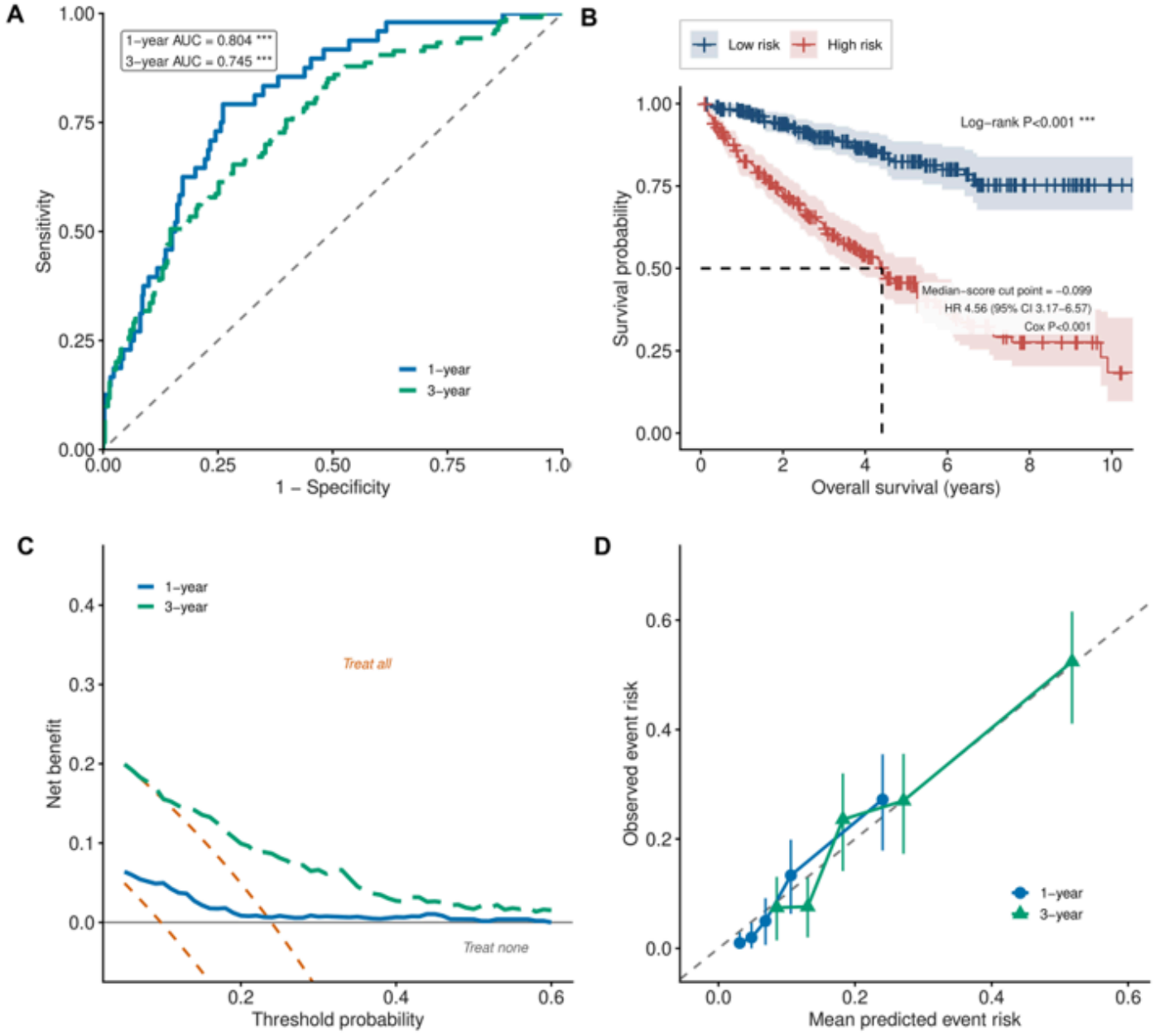


Figure 4

Apparent performance of the historical frozen TRIM-8RS in the TCGA-KIRC development cohort (n=508; 171 deaths). A Inverse-probability-of-censoring-weighted time-dependent receiver operating characteristic curves at 1 and 3 years. Areas under the curve were 0.804 and 0.745, respectively. B Kaplan-Meier overall-survival curves for groups defined by the frozen TCGA median score cutoff of −0.099. Shaded areas indicate 95% confidence intervals; the high-risk versus low-risk hazard ratio was 4.56 (95% confidence interval, 3.17–6.57), with Cox and log-rank P<0.001. C Inverse-probability-of-censoring-weighted decision-curve analysis at 1 and 3 years, comparing TRIM-8RS with treat-all and treat-none strategies over threshold probabilities of 0.05 to 0.60. D Quintile-based calibration plots of mean predicted event risk against observed 1-Kaplan-Meier risk; error bars indicate 95% confidence intervals and the dashed line indicates ideal calibration. Because TCGA-KIRC was used to construct the

historical score, these are apparent development-cohort results rather than independent validation. ***P<0.001 versus 0.50. Data source: TCGA-KIRC, Genomic Data Commons.

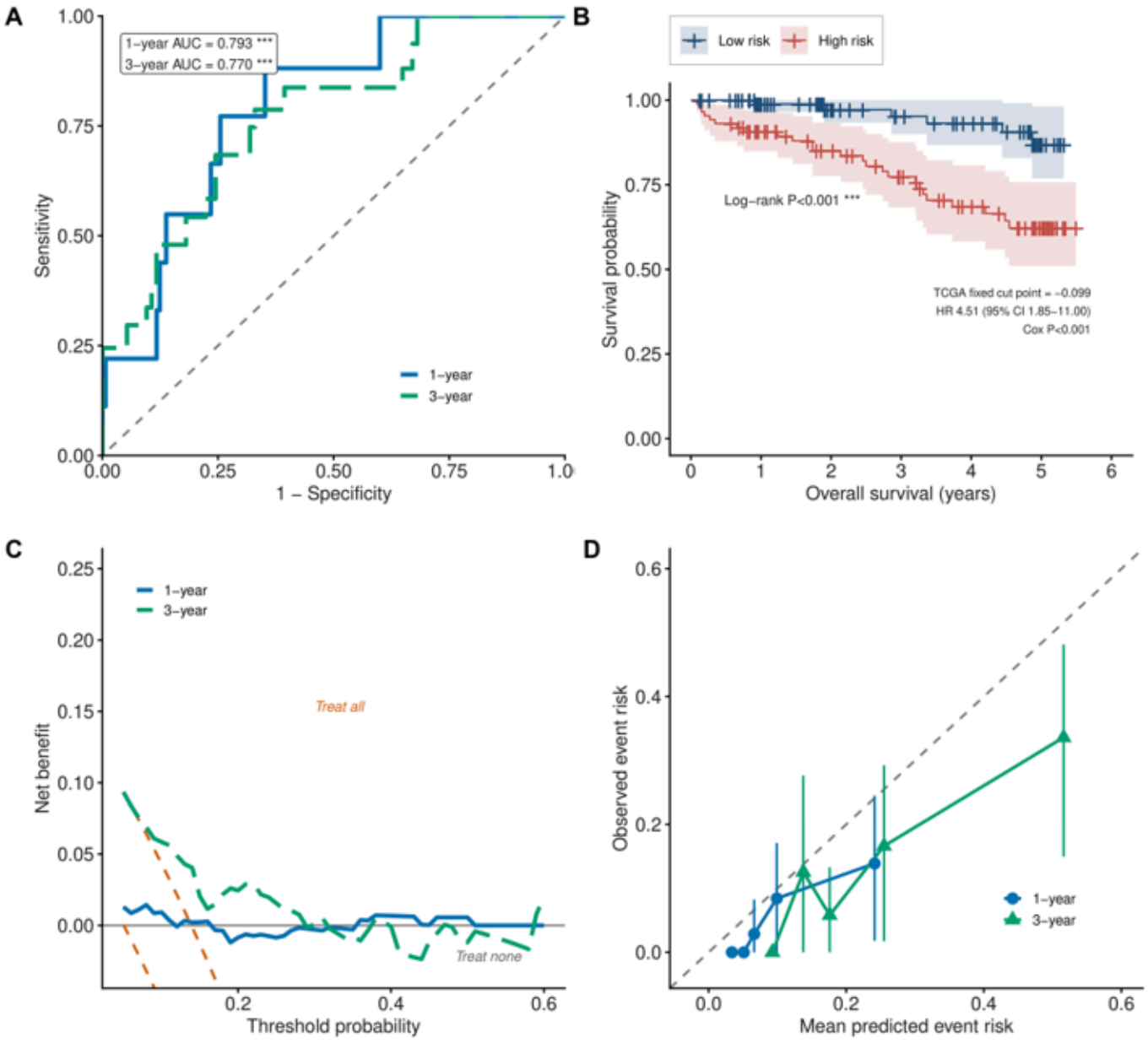


Figure 5

External evaluation of the historical frozen TRIM-8RS in the CPTAC operational primary-RCC RNA-sequencing cohort (n=183; 31 deaths). A Inverse-probability-of-censoring-weighted time-dependent receiver operating characteristic curves at 1 and 3 years. Areas under the curve were 0.793 and 0.770, respectively. B Kaplan-Meier overall-survival curves for the 96 low-risk and 87 high-risk patients defined with the fixed TCGA score cutoff of −0.099. Shaded areas indicate 95% confidence intervals; the high-risk versus low-risk hazard ratio was 4.51 (95% confidence interval, 1.85–11.00), with Cox and log-rank P<0.001. C Inverse-probability-of-censoring-weighted decision-curve analysis at 1 and 3 years. D Quintile-based calibration of frozen 1- and 3-year event risks against observed 1-Kaplan-Meier risk. TCGA

coefficients, the score cutoff and the baseline hazard were fixed before CPTAC outcome evaluation. CPTAC was analyzed as an operational primary-RCC cohort rather than a uniformly pathology-curated clear-cell RCC cohort; its limited event count warrants cautious interpretation of absolute-risk calibration. ***P<0.001 versus 0.50. Data source: CPTAC-3 Kidney, Genomic Data Commons and cBioPortal.

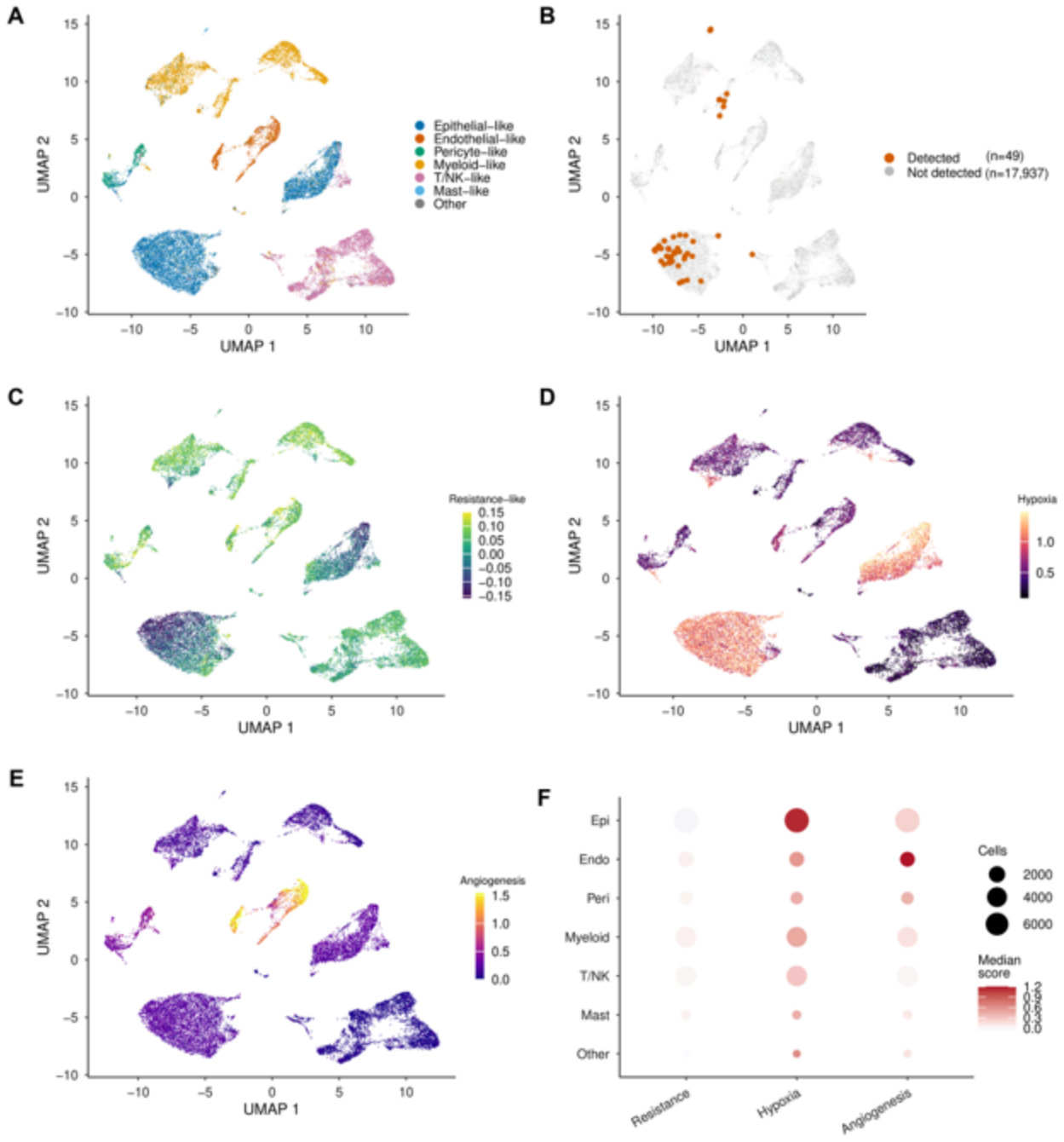


Figure 6

Single-cell localization and state summaries in two ccRCC specimens from GSE152938. After quality control, 8,873 ccRCC1 cells and 9,113 ccRCC2 cells were retained. A Uniform manifold approximation and projection colored by conservative cell-compartment annotation. B Uniform manifold approximation

and projection showing raw TRIM63 detection, with 49 TRIM63-detected and 17,937 undetected cells. C–E GSE64052-derived resistance-like, hypoxia and angiogenesis scores, respectively. F Median state scores by cell compartment; point size indicates the number of cells. These scores are transcriptomic state summaries and are not measured sunitinib-response labels. All 49 TRIM63-detected cells had one raw UMI. Data source: GEO series GSE152938, samples GSM4630028 and GSM4630029.

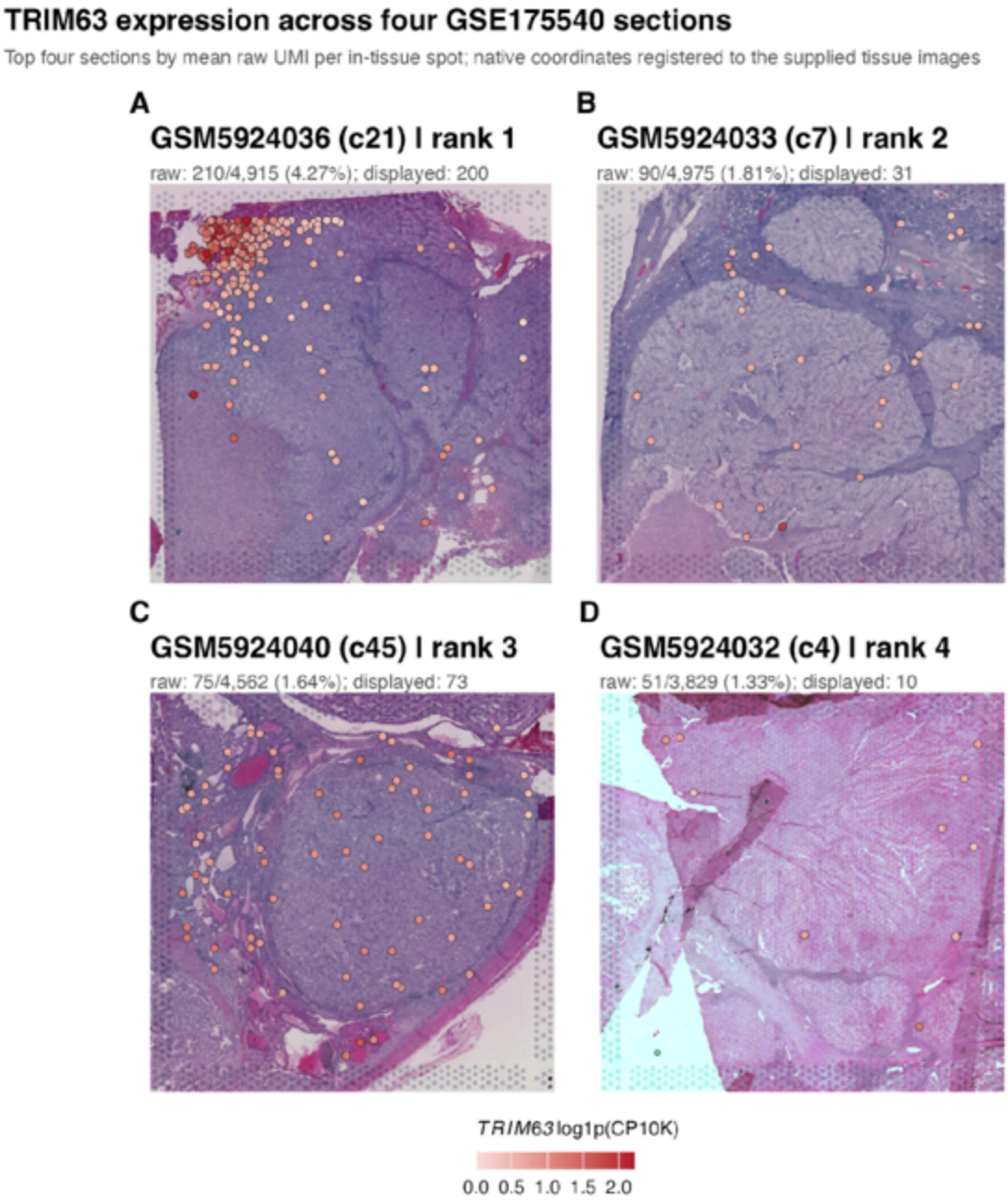


Figure 7

Tissue-registered display of TRIM63-positive spots in GSE175540 spatial-transcriptomic slides. All 11 available slides were ranked by mean raw TRIM63 UMI per in-tissue spot. A GSM5924036_ffpe_c_21, rank 1: 210/4,915 raw-positive spots (4.27%), of which 200 were displayed. B GSM5924033_ffpe_c_7, rank 2: 90/4,975 raw-positive spots (1.81%), of which 31 were displayed. C GSM5924040_ffpe_c_45, rank

3: 75/4,562 raw-positive spots (1.64%), of which 73 were displayed. D GSM5924032_ffpe_c_4, rank 4: 51/3,829 raw-positive spots (1.33%), of which 10 were displayed. Colored spots had raw TRIM63 UMI >0 and passed the prespecified strict-display criterion of at least 0.50 overlap with a per-slide optical-density Otsu tissue mask; color denotes TRIM63 log1p(CP10K [counts per 10,000]) on a common scale. Raw-positive counts were retained for quantitative detection, whereas the mask was used only for visualization quality control and was not a pathology annotation. No smoothing or imputation was applied. The maps do not assign TRIM63 to a cell type or pathological region and do not support a treatment-response association. Data source: GEO series GSE175540.

Supplementary Files

This is a list of supplementary files associated with this preprint. Click to download.

- SupplementaryFigureS1.tiff